THE ISOCAM CALIBRATION ERROR BUDGET REPORT

A. Biviano[1,2]

1: Osservatorio Astronomico di Trieste, via G.B. Tiepolo 11, I-34131 Trieste, Italy
2: CAM IDT, ESA Satellite Tracking Station, PO Box 50727, E-28080 Madrid, Spain

Version 3.1 – August 14^{th}, 1998

Abstract

In this document we give a description of the sources of error in the CAM calibration at the present state of knowledge and understanding. An error budget is established on the basis of the results derived from the data obtained from the calibration observations performed during PV Phase and Routine Phase.

We provide a list of the instrumental effects contributing to the error budget, and compare current estimates of the magnitude of these effects to pre-launch estimates; generally, a good agreement is found.

1 Introduction

In this document we try to establish the error budget of the CAM calibration, based on calibration observations performed during the whole ISO mission. We refer to several technical reports that have been (or are being) produced, where the interested reader can find all detailed information on the calibration data-sets used, and the analysis performed. Only in a few cases, we thought it important to expand this presentation beyond a simple summary of existing documents, either because the documents do not exist yet, or because the available information is spread out in too many reports (§ 2, § 5, § 11, § 12),

The reader will notice that the CAM LW detector error budget is better constrained than the CAM SW detector one. This is due to the larger effort put into calibration and understanding of the LW detector. However, let us stress that the fraction of time spent into calibration and understanding of the SW detector is nevertheless much larger than the fraction of CAM observing time that observers have chosen to dedicate to the SW detector (~ 3 % only).

A comparison of the current estimates of the magnitude of all the error sources affecting the CAM calibration, with pre-launch expectations, is done in § 13. In general, good agreement is found.

A table summarising this document is given in § 13. While the impatient reader would skip all these sections and refer to Table 4, we recommend not to do so, because a single value in a table has little meaning if it is not accompanied by a detailed explanation of how it was derived. However, the same table is certainly useful as a quick-look reminder.

2 Glitches and transients

It is generally accepted that the most important noise sources in the CAM observations are the cosmic ray impacts (glitches), and the slow response of the detector to flux variations (see, e.g. Starck et al. 1998). This was actually understood long before the ISO launch (see, e.g., Pérault et al. 1994).

Understanding the behaviour of the stabilization and the effect of glitches on the detector is essential for properly correcting for related effects. Modelling of these effects can be done (and has been attempted) on the basis of the pre-launch knowledge of the detector, and of in-flight measurements.

It is customary to distinguish among three kinds of glitches, usually called *common, faders* and *dippers* according to their behaviour, decay time and influence on the pixel responsivity (see Claret & Dzitko 1998). It is likely that common glitches are physically associated to impacts of cosmic ray electrons, while faders and dippers are linked to impacts of proton or α particles (see Aussel et al. 1998).

Typically, common glitches only last few readouts, and the decay time is more or less as fast as the rise time. These are easy to remove, and contribute to the noise in the CAM images only because the frames affected by these glitches cannot be used. Based on the observed average glitch rate and the average number of pixels hit by a glitch (see Claret & Dzitko 1998), one can estimate that every pixel will be hit by at least one glitch every $\simeq$ 120 s. Thus, using an integration time T_{int} of 2.1 s, one frame out of 60 will be lost on average. On the other hand, using longer integration times, e.g. T_{int} =10 s, one frame out of 12 will be lost. Since the signal-to-noise (s/n) in the case of Poisson noise is simply proportional to the square root of the number of frames, we see that even with T_{int} =10 s, loosing one every 12 frames only reduces the s/n by 5 %. This is consistent with pre-launch expectations (Pérault et al. 1994).

On the other hand, faders and dippers have a much longer lasting impact on the pixel sensitivities. Faders are followed by a slow decrease of the signal, while dippers are followed by a reduction of the sensitivity of the pixel, that recovers very slowly afterwards (see figures in Claret & Dzitko 1998). In these cases, the number of affected frames is much higher, the sensitivity of the pixel taking from tens to hundreths of seconds to fully recover. Fortunately, faders and dippers occurr less frequently than common glitches (two orders of magnitude less frequent) so that even if they affect more frames, the global s/n of the final image should not be severely affected. Note that this is true only if all the affected frames are masked in the data-reduction. Usual deglitching routines in the CAM Interactive Analysis (CIA; Ott et al. 1996, Delaney 1997) software package, only mask the frames corresponding to the glitches, so that a visual inspection of all pixel time histories is needed for a proper masking (or the use of more clever algorithms, such as those developed by Lari 1997 and Starck et al. 1998).

The impact of faders and dippers on pixel sensitivities is related to the general problem of the transient behaviour of the CAM detector. That the time constants appearing in the detector response to flux variations, were very long was known since pre-launch calibration (Pérault et al. 1994; see also the "ISOCAM Observer's Manual"). The time constants are different for different flux steps, and for different pixels. Note in particular that it takes longer for the signal to stabilize after a given flux step, if it happens above a background of lower flux. Pixel coupling may be a further complication, when the array has a non-uniform illumination.

We can identify several kinds of errors induced by transients:

- flat-fielding noise, because different pixels in different illumination conditions have different stabilization behaviour (see also Biviano et al. 1998a); in particular the apparent background flux in a raster image is changing from one image to another;
- creation of ghost images, appearing in positions of the array that have seen a strong

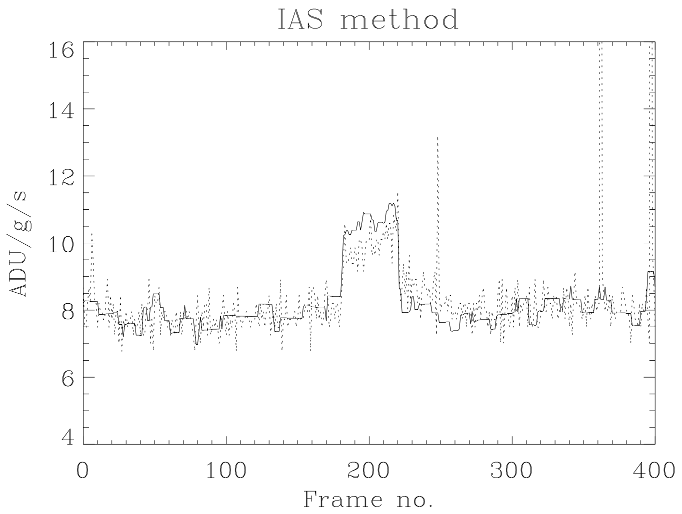

Figure 1: Flux (ADU/g/s) vs. frame for a single pixel. A source is seen during an LW2, T_{int} =2 s, 6″PFOV, 3×3 raster observation. Dotted line: raw data (after dark subtraction); full line: IAS-method corrected data (after dark subtraction and deglitching).

source, that left a remnant memory;

- general increase in the noise level, because of the transient behaviour following the glitch impacts;
- systematic error in the photometry, because both the background and the source observed fluxes differe from the true ones in case of not complete stabilization.

Curing operations, such as cleanup flashes or photon showers from the internal calibration device (ICD hereafter) have severe drwabacks on photometric and flat-field (FF hereafter) accuracies, so that the best solution for recovering the true flux from a not stabilized transient behaviour lies in a proper data-reduction analysis. Possible solutions are:

1. guessing which are the stabilized values and rejecting non-stabilized frames in the analysis;
2. identifying sources over a variable background;
3. correcting the not stabilized pixel signal, according to a given model.

The first solution is the simplest one, and it is adopted in the CIA routines *S90,* and *KSIG.* However, the case when the signal is not stabilized is very frequent, and even rejecting most of the frames does not help in revovering the true incident flux if the signal is *not* stabilized in any frame.

The second solution is implemented in the PRETI method (Starck et al. 1998), not yet available to the whole community. The method is extremely succesfull in identifying sources over a variable background, and to correct for glitches and glitch effects on the pixel sensitivities. However, it is not suited for recovering the systematic photometric errors.

The third approach is the one adopted by Abergel et al. (1996, hereafter referred as "the IAS method"), Acosta (1998), and Lari (1997). The first two methods have two transient components, one accounts for the immediate response of the detector, and the other for the fast response. Lari's method includes one additional component, that accounts for the slow response of the detector. This component is essential in recovering the transient effects of the dippers, as it can be seen by comapring the results of the transient corrected time histories of a pixel, using the IAS method or Lari's routine.

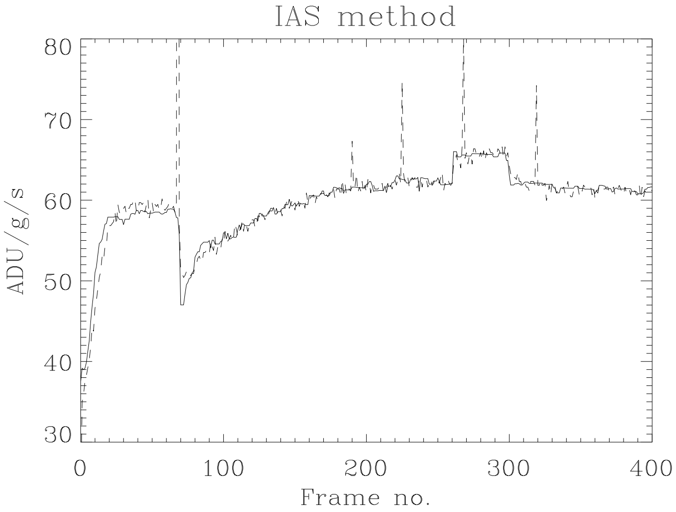

Figure 2: Flux (ADU/g/s) vs. frame for a single pixel. A source is seen during an LW10, T_{int} =2 s, 6″PFOV, 3×3 raster observation. Dashed line: raw data (after dark subtraction); full line: IAS-method corrected data (after dark subtraction and deglitching).

Note that these methods apply for the moment only to the CAM LW detector, not to the SW one.

In the example shown in Fig. 1 we can see the illumination history of a pixel that sees a source during a raster observation. The observation is an LW2 (reference wavelength $\lambda = 6.7\mu$m, see Blommaert 1998) 3×3 raster, at integration time T_{int} =2 seconds ("s" hereafter), and 6″pixel field-of-view ("PFOV" hereafter). The target source, a giant galaxy at the centre of a nearby cluster, is seen by this pixel only at the central raster position (around frame 200). The raw (dark-current subtracted) data (dotted line) show an initial flux step over a stabilized background, when the source first illuminate the pixel, followed by an upward stabilization, and an exponential decrease when the satellite moves to the next raster position. The full line shows the flux recovered using the IAS method (after dark-current subtraction and deglitching). It is clear that a significant part of the source flux would have been missed, had the raw data not been corrected.

In Fig. 2 we show another pixel illumination history. The observation is an LW10 (reference wavelength $\lambda = 12\mu$m, see Blommaert 1998), 3×3 raster, T_{int} =2 s, and 6″PFOV, on the same target as before. In the raw (dark-subtracted) data (dashed line) one can notice an upward stabilization of the background flux, followed by a dipper, that has the effect of strongly decreasing the responsivity of the pixel itself. After the dipper impact, there is a long upward flux transient, lasting $\sim$ 150 frames. During the transient, two common glitches hit the pixel, without consequences for the pixel responsivity. Around frame 260, the source first illuminate the pixel, and induces a flux step, followed by an upward transient, that reaches stabilization before ISO goes to another raster position (another common glitch hits the pixel in the meanwhile, but this does not affect the upward transient behaviour). The full line represents the flux recovered using the IAS method (after dark-current subtraction and deglitching).

By comparing Fig. 1 with Fig. 2, one can immediately note that the source photometry is less affected by transient effects in the LW10 observation than in the LW2 one, despite the flux step is similar ($\simeq$ 4 Analog-to-Digital Units, divided by the gain factor, g, and the

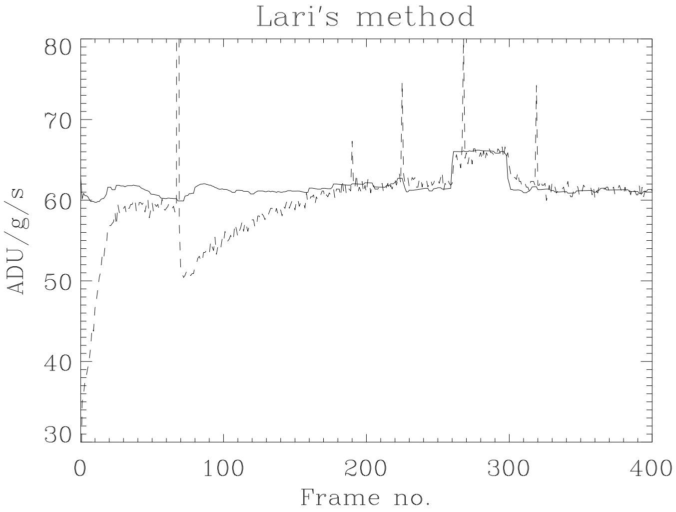

Figure 3: Flux (ADU/g/s) vs. frame for a single pixel. A source is seen during an LW10, T_{int} =2 s, 6″PFOV, 3×3 raster observation. Dashed line: same raw data as in Fig. 2; full line: Lari's method corrected data (after dark subtraction and deglitching).

integration time, T_{int} =2 seconds, "ADU/g/s" hereafter[1]) in the two cases. This happens because the same flux step induces a faster transient when it happens over a higher flux background (see, e.g., "ISOCAM Observer's Manual", and the equations in Abergel et al. 1996 and Lari 1997).

While the IAS method is able to recover the source flux lost because of incomplete stabilization, it fails in recovering the long timescale transients, as is clear from the fact that the dipper effect is not corrected at all (see Fig. 2). This is not surprising, since the current version of the IAS method only has two transient components. Including a third (slow) component allows to do a much better correction. This is illustrated in Fig. 3, where the same raw data of Fig. 2 are shown (dashed line), but this time the full line represents the flux recovered using Lari's method (after dark-current subtraction and deglitching). Despite some irregularities (that can be reduced by pushing the accuracy of the method, at the expense of an increased computing time), it is clear that *all* the transient behaviours are now corrected. Not only is the source photometry recovered (in quantitative agreement with the IAS method), but also the initial upward transient of the background flux, and the upward transient following the dipper, are recovered.

While Lari's method proves superior to other methods in this case, a current limitation of Lari's method is its long computational time, mostly due to the fact that the model parameters (such as the time constants for the fast and the slow component), at variance with the IAS method, are not fixed, but fitted to the data (see Lari 1997 for further details).

Only a limited set of data have by now been reduced using Lari's method of transient corrections, because this method only became available quite recently. Results of a comparison of Lari's method with the IAS method for a limited set of observations is given in Table 1.

Note that data-reduction with *S90,* and *KSIG* has not been considered, since the result of these routines is very much dependent on the kind of observations. It is clear that since these routines mask out all non-stabilized frames, they make the *a priori* assumption that

[1]FF measurements are sometimes done with a gain factor ×1, and sometimes with a gain factor ×2. Here and in the rest of this document, all units are scaled by the gain factor *even if not explicitely indicated* – i.e. both "ADU" and "ADU/g" mean Analog-to-Digital Units scaled by the gain factor.

Table 1: Transient correction methods

Method	Source name	Source flux (ADU/g/s)	Per pixel background flux (ADU/g/s)	Per pixel background RMS (ADU/g/s)
IAS	MS2137-1	0.19	0.52	0.003
LARI		0.21	0.52	0.002
IAS	MS2137-2	0.13		
LARI		0.13		
IAS	MS2137-3	0.15		
LARI		0.11		
IAS	A2877 cD	70.7	59.5	0.35
LARI		61.2	60.0	0.15
IAS	HIC96062	6.4	0.20	0.025
LARI		4.8	0.20	0.023
ACOSTA		6.7		

at least one stabilized frame exists. This is far from true in general, unless the observations last very long, like in the case of calibration observations. Even for calibration observations, however, it has been shown that full stabilization is not always achieved (Blommaert 1998, Biviano et al. 1998a).

From the results in Table 1 it can be seen that while Lari's method allows to reach a better s/n, it tends to give lower flux estimates than the IAS method (by $\sim$ 10 %, on average). Globally, the two methods provide consistent results within $\pm$15 %. This is reassuring, since most calibration data-reduction has been done using the IAS method (since it was the first reliable stabilization-correction method to become available for use within the CIA).

It is clear, however, that there exist problematic cases that are not correctly handled by all methods, e.g. when a pixel sees a source while the pixel flux is stabilizing upward (at the beginning of a raster, or after a dipper), or when the pixel is hit by a dipper while it is illuminated by a source. An example of the last case is shown in Fig. 4: the raw data (after dark-current subtraction, dotted line) show a dipper impact on a pixel while the pixel was being illuminated by the target source. The dipper affects the pixel responsivity, and this affects the flux one would deduce for the source. Using the IAS method for correcting the transient (dashed line) does not help much, since the method cannot account for the long term transient effect after the dipper. On the other hand, Lari's method is able to fully correct the illumination history of the pixel, both the flux step due to the source, *and* the dipper-induced transient.

In this specific case, using the IAS-method one would fall short of $\sim$ 30 % of the flux estimated with Lari's method. However, due to the point-spread-function ("PSF" hereafter), even a point source will be normally imaged by several pixels, so that the *total* flux of target source would be normally less affected than the flux on a single pixel[2].

Our conclusion is therefore that the currently available understanding of the transient behaviour of the LW CAM detector, and the currently available methods for deglitching and transient correction, allow to reach a level of $\sim$ 15 % accuracy or better in photometry, and

[2]This consideration is valid only to a certain extent, as it is often the case that neighboring pixels are affected by the same glitch.

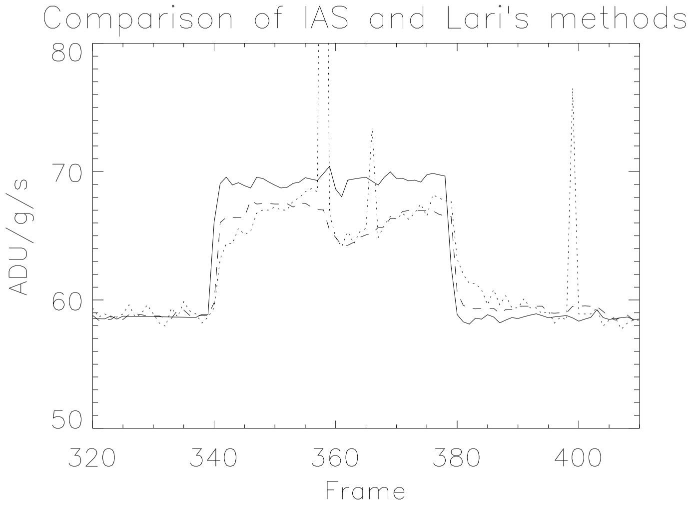

Figure 4: Flux (ADU/g/s) vs. frame for a single pixel. A source is seen during an LW10, T_{int} =2 s, 6″PFOV, 3×3 raster observation. Dotted line: raw data, after dark subtraction; dashed line: IAS method corrected data; full line: Lari's method corrected data.

to improve by a factor ≥ 2 the s/n of an image. This is not a free lunch, however, since an accurate (and time-consuming) data-reduction is needed.

3 Saturation

We refer to Gallais (1996) for a detailed overview of this topic. Let us summarize here part of this document, and add some considerations.

Saturation of the detector may be considered as an extreme example of a long transient behaviour induced on the detector pixels. A basic difference between saturation-induced transients and those induced by a change of illumination or a glitch hit, is that when saturation occurs the photometric information on the incoming flux is lost. It remains to be seen if the transient correction methods described in § 2 can help in this case.

Since saturation is an unwanted (and dangerous) event for the CAM detectors, no on-purpose saturating observations have been done for calibration purposes. However, few saturation events occasionally occurred during the ISO mission. The effects of saturation occurring during a given revolution could often be seen in the deactivation FFs (Gallais 1998). This allowed to show that the pixel responsivities can decrease by ≥ 30 % following a saturation events. Most importantly, this loss of responsivity following a saturation may last for several hours.

The considerable impact of saturation on the detector responsivity fully justify the large amount of time spent by CIDT and SOST to screen the POFs and pre-screen the Mission-Data-Base for identification of dangerous observations for observations with CAM (both in prime and in parallel mode). This screening has made the occurrence of saturation a very rare event.

4 Readout

The readout noise has been estimated before launch to be $\simeq$ 180 e^- per-pixel RMS, and $\simeq$ 700 e^- per-pixel RMS, respectively, for the LW and SW detectors ("ISOCAM user's

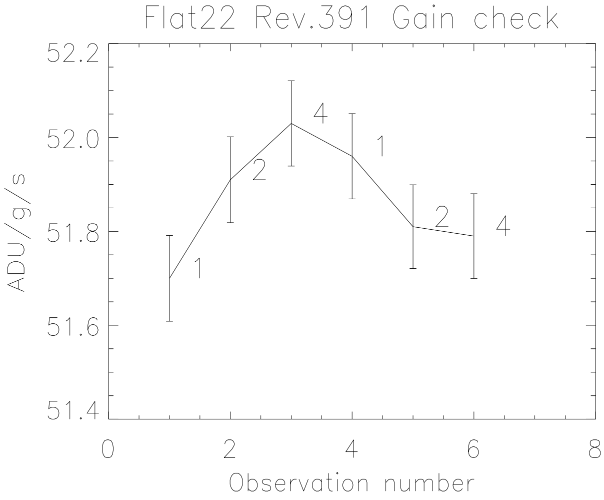

Figure 5: The average flux over the whole array for different gains.

Table 2: Gain measurements

Gain	Average signal (ADU/g/s)
1	51.83 ± 0.09
2	51.86 ± 0.09
4	51.91 ± 0.09

manual"). This converts to 0.7 ADU/g and 2 ADU/g RMS, respectively.

5 Gain

During revolution ("rev." hereafter) 391, an empty region of the sky was imaged in LW10, with the $3''$ pixel-field-of-view (PFOV hereafter) and integration time (T_{int} hereafter) of 5.04 s, using the three different gains available for the LW CAM detector. The gain was changed from 1 to 2 to 4 and then again to 1, 2 and 4, sequentially; 179 frames were taken per each gain observation. The sequence was repeated twice for reducing the systematic error due to incomplete stabilization. As the gain is unique for all pixels, after the usual data-reduction, we only considered a global value of the signal over the array, i.e. the mean (or the median) of all pixel values, for each observation.

In Fig. 5 we plot the average of the measured signal over all pixels for each observation. The signal level does not seem to be constant, but this is probably due to a stabilization trend. By averaging the values obtained in different observations done with the same gain, we find the values listed in table 2. The differences among the values obtained with different gains are within the error bars, and the maximum difference is 0.15 %, which sets the accuracy level of the gain.

6 Darks

We refer the reader to Biviano et al. (1998b) for a detailed description of all aspects of calibration concerning the CAM dark-current. Here we summarize their conclusions for what concerns the error-budget.

Biviano et al. have shown that the LW detector dark-current depends linearly on the rev. number, in a slightly more complicated way on the time of the observation within a given revolution, and again linearly on the detector temperature.

More specifically, the dark-current drift from the beginning to the end of the ISO mission is ~ -2 ADU, the dark-current drift within each single revolution, from the activation to the de-activation of the CAM instrument, is $\sim \pm 0.5$ ADU (the drift can be positive or negative for different pixels), abd the temperature-dependence is ~ 0.5 ADU for the full range of detector temperature variation (a few hundreths of a kelvin).

These dependencies are far from negligible, and they would affect the final accuracy that can be reached with dark-current subtraction. Fortunately, a modellisation of these effects has been done, and it is already available in CIA and Off-Line Processing (OLP; Siebenmorgen et al. 1998). Using the dark-current model allows to reduce the per-pixel residual from dark-current subtraction, to $\simeq 0.25$ ADU/g, on average, i.e. two times lower than what could be achieved early in the ISO mission, when a simple average of several dark-current measurements was used.

For what concerns the SW detector, none of these dependencies has ever been observed, so that the dark-current subtraction is still based on a simple average of several dark-current measurements. The per-pixel residual from dark-current subtraction is in this case $\simeq 0.5$ ADU/g.

These values are derived by comparing several dark-current images, and are therefore *external* RMS estimates of the per-pixel dark-current noise. Based on the number of frames used for constructing a single dark-current image, it is easy to show that these external RMS noise estimates are close to the theoretical estimates one expects from readout noise only (see § 4).

7 Flat Fields

We refer the reader to Biviano et al. (1998a) for a detailed description of all aspects of calibration concerning the CAM flat-fields. Here we only summarize their conclusions for what concerns the error-budget.

Biviano et al. have shown that the accuracy with which we can derive FFs on the sky is either limited by incomplete stabilization, or by the low zodiacal background flux level, in which case the dominant source of error is the dark subtraction, and, in the end, the readout noise (see § 6).

Beating the stabilization noise by integrating longer was shown to be impossible, because of observing time limitations. The use of transient-correction models (see § 2) could help only if these models include a long timescale transient component. This is worth trying in the post-operational phase.

Whenever the zodiacal background flux was too low to allow a proper characterization of the FF in a given configuration, alternative flat-fielding strategies have been considered, such as using the internal calibration device ("ICD" hereafter), or the FF obtained in another filter. The noise introduced by these alternative methods is small enough that they can be considered valid.

The accuracy of calibration FFs depends very much on the configuration, and it increases with the wavelength, the width of the filter, and the PFOV, but it may drop at the edge columns of the CAM LW detector, due to the lens wheel jitter (see § 12).

The most important source of error induced by flat-fielding is the background noise; identifying faint sources over a high background requires a very accurate FF. We can therefore characterize the CAM FF accuracy by the that of the configuration with the highest background flux, i.e. the LW10 filter at 6″PFOV (let us neglect here the 12″PFOV, since it is seldom used by observers). The calibration FF for this configuration is accurate to $\simeq 0.5$ %; this induce a background RMS of 0.25 ADU/g/s for an average sky brightness of 50 ADU/g/s.

Anyway, it must be stressed that most raster and beam-switch CAM observations provide their own FF, and need not be particularly concerned about the quality of the calibration FFs.

8 Photometry

8.1 Calibration sources

In this section we estimate the error budget of the photometric measurements done for calibration purposes. We refer to Blommaert (1998) for a full description of the photometry on point-sources performed to establish the calibration of the CAM filter sensitivities. Note that photometry with the circular variable filters ("CVF" hereafter) is described in § 10. Photometry involves of course many aspects of the CAM calibration, such as the dark-current, the flat-fielding, the PSF, the effects of glitches and transients, the straylight, etc. As many of these aspects are dealt with in separate sections of this document, they will not be repeated here.

Here we mainly summarize some of the results from Blommaert (1998). Since the photometric measurements are usually done on bright stars, our conclusions cannot be immediately extended to the topic of faint-source photometry (see § 8.2).

The main purposes of photometric calibration are to provide the user with the conversion factor (called "sensitive factor") from instrumental units (ADU/g/s) to physical units (Jy), appropriate to any given filter, and to check for any dependence of these factors on temporal variables, and spectral shapes of the calibration sources.

Blommaert (1998) has shown that repeated photometric measurements of several calibrating stars converge to sensitiv factors that are very close to the pre-launch values ("ISOCAM observer's manual"), except for the SW filters, for which however the pre-launch values are known to be wrong (an inverse dependence on the λ was missing). Once the pre-launch SW sensitiv values are corrected, the most discrepant values are found for the LW1 and LW9 filters; the pre-launch sensitiv values are 15 % higher. Since the sensitiv factors are accurate to $\simeq 5$ %, these differences are significant. A possile explanation for the LW1 filter sensitiv factor discrepancy comes from the difference between the theoretical PSF (used to derive the in-orbit estimation of the sensitiv factor) and the observed one (see § 9). At the time of this writing, the discrepancy of the LW9 filter pre-launch and in-orbit sensitiv factors, is unknown.

Part of the RMS in the sensitiv values may come from a systematic decrease of the responsivity detector through the orbit, $\simeq -6$ % from activation to de-activation, i.e. $\simeq -0.4$ % per hour. Note that this decrease in sensitivity has been deduced by repeated observations of the same star at different times in the same revolution. However, it has also been seen in the long zodiacal background observation of rev.22, where the flux has been found to decrease from an apparently stabilized value reached after 5500 s of observing time, by ~ 0.5 % in the next 1.2 hours, in perfect agreement with the trend found above.

On the other hand, no long-term responsivity trend has been detected through the ISO mission.

What is the source of the sensitiv factor RMS? The decrease of responsivity through a revolution cannot account for all the sensitiv factor RMS. The calibration stars are too bright for the read-out and dark-current noise to have any impact on their photometry. Different deglitching methods can in principle modify the photometry of a bright star by several percents. However, Blommaert (1998) has consistently reduced all the data with a single deglitching routine. Flat-fielding errors are likely to be small, because the source image is always located at the centre of the array, where the flat-fielding accuracy is of order 1–2 % at most. The source position on the detector or in different parts of a pixel does not affect the photometric measurements by more than 3 % (see § 9 and Okumura 1998a).

While all these effects could sum up to the observed 5 % RMS, it is likely that most of the sensitiv value RMS is due to incomplete stabilization of some observations.

8.2 Faint sources

TBW.

9 Point Spread Functions

A full description of the PSF calibration observations and its applications, is given in Okumura (1998a). As a consequence, here we only provide a very concise summary of Okumura's results.

The PSF measurements are done (mainly) with two purposes:

1. deconvolution;
2. normalising factor for photometry correction.

However, it must not be forgetten that PSF measurements are also a valid data-base for transient studies, straylight, and photometry.

Since very early in the ISO mission, a 15 μm PSF image been available, showing the Airy pattern down to the sixth Airy ring. However, even this very impressive result may not reach the required accuracy for what is known to be an extremely difficult task, i.e. deconvolution. Indeed, despite a large effort in observations and data-reduction techniques, the characterization of the deconvolving profile does not yet reach the accuracy needed for building a robust deconvolution method. The reason lies in the insufficient sampling of the ISOCAM images, the limited ISO pointing accuracy, and the different stabilizing behaviour of different pixels. However, the analysis is ongoing and new tools are being developed for improving the deconvolution accuracy. The method developed by Laurent et al. (1998) is applicable only to bright point-like sources.

Pre-launch tests suggested that the PSF could be expected to vary significantly over the detector array, and that it would depend upon the precise position of the source on a pixel. In the light of the expected significant implications for photometric accuracy, especially for point sources, an extensive programme of PSF measurements over the field-of-view and throughout the optical parameter space, was planned and has been executed, since launch. However, in-orbit observations of the ISOCAM PSFs have shown that the normalising factors vary by 2–3 %, and this variation is within the accuracy achieved with the PSF measurements, so that it cannot be considered significant. Only the $12''$PFOV PSF show a large dispersion (≤ 40 %) of the normalising factors of different locations on the detector array. This is due to ghost images and residual vignetting effect after flat-fielding.

As discussed in Blommaert (1998) and Biviano et al. (1998c), the filter and CVF responsivities are obtained by correcting the aperture photometry using the theoretical ISOCAM

PSF. It is then important to know how well does the theoretical PSF approximates the observed ones. Okumura shows that they compare very well, except for cases (mainly at 12″PFOV and with the CVF) when the ghost contribution is important, and for the LW1 filter, that has a wider PSF than expected. The reason for this discrepancy is not understood at present, but it is clear that it does not come from the telescope performance (since the observed PSF in an SW filter of similar wavelength does not show such a discrepancy).

The PSF correction for photometry may be quite important. If the source image is located at the centre of the array, and the background is estimated from the edges of the image, at 1.5″PFOV, one would loose up to 11 % of the source flux, if no PSF correction is neglected. The correction is even larger when the source image is at the edge of the array (e.g. 21 % in the LW9 filter when the source image is located at position (4,4)).

10 CVF

All aspects of CVF calibration are detailed in Biviano et al. (1998c). Let us here summarize their results.

The comparison between the CVF spectral response functions ("SRF" hereafter) measured pre-launch and in-orbit, show clear discrepancies. The reason for the difference is due to an error done in the pre-launch SRF for what concerns the SW CVF SRF. Once this error is corrected, the average difference between the pre-launch and in-orbit SRFs is only ~ 1 %. On the other hand, the in-orbit LW CVF SRF is (on average) 0.8 times the pre-launch one, and the difference is attributed to the flux lost into ghost images. Indeed, the the calibrating star observations have been reduced by taking care of *excluding* the contribution of the ghost to the source flux. This choice assures consistent photometry at different PFOVs, because the ghost is visible only in the 6″LW CVF images, as it falls outside the array at smaller PFOVs. Further details on the ghost effects in CVF observations are given in § 11.

Apart from the systematic error arrising from ghost images, when the photometry is done in the same way, the measured SRFs are very accurate. The RMS of several measurements of the SW SRF is 3 % (average over all the CVF steps), same as the RMS of the LW CVF1, while the RMS of the LW CVF2 is a little bit higher (4 %). On the other hand, the SRF of the long-wavelength LW CVF2 positions have much larger uncertainties (~ 20 %), but these positions are not recommended for use (see the "ISOCAM user's manual"). Biviano et al. show convincingly that the main source of error in the SRF is stabilization noise.

Once the SRF is established, one can address the issue of absolute flux calibration. Cross-calibration between CAM CVF and other instruments indicates that (for bright stars) the absolute flux calibration of the CVF is correct to within 2 %. It is clear, however, that ghost images can affect photometry to a much higher level (20-30 %, see § 11).

The wavelength calibration of the CVF is also well established. When the source image is located at the centre of the detector, the wavelength calibration is accurate to within a tenth of a CVF step. However, there is a wavelength dependence with the column position of the source image (and no dependence with the line position); when the source image is located at the left edge of the array, there is a wavelength shift of up to +1 CVF step position (depending on the wavelength).

11 Straylight and ghosts

Straylight and ghosts occur in the ISOCAM instrument under a variety of conditions. To a great extent this problem was anticipated before launch and is expected to be internal to CAM and related to detector-lens and detector-CVF reflections. While this is not a problem which threatens the usefulness of the camera, it is however one which demands great caution of observers when interpreting data on high-contrast sources and it represents one of the more difficult-to-characterise aspects of CAM behaviour.

Ghost-images are particularly important in CVF (Biviano et al. 1998c). This was expected since, at variance with CAM filters, the CVF could not be tilted with respect to the optical axis. However, the presence of ghost can also be seen very clearly in many CAM filters at 12″and 6″PFOV (Okumura 1998a,b), since the filter tilt is not always sufficient to displace the ghost reflection off the detector.

Following Biviano et al. (1998c), we can distinguish two kinds of ghosts: the *comoving* ghost and the *symmetric* one. The former is located close to the source image, with a small displacement. The latter is instead located on the array at a position roughly symmetrically opposed to the position of the source, with respect the centre of the array. Okumura (1998b) refers to the two types of ghosts as the *primary* and the *secondary* ghost, respectively. Other ghosts are probably present but remain undetected because they contain a minor fraction of the source flux.

The two kinds of ghost have different fluxes and different origin. The primary/comoving ghost arises from a first reflection on the plane of the detector, followed by a second reflection on the surface of the filter. Its integrated flux is $\sim$ 20-30 % of the source flux (Biviano et al. 1998c, Okumura 1998b). The secondary/symmetric ghost is generated by a double reflection on the same surfaces as the primary ghost (Okumura 1998b), and contains $\sim$ 5-10 % of the source flux (Biviano et al. 1998c, Okumura 1998b). The integrated ghost fluxes are generally larger in CVF images than in filter images. The ghost spectra are very similar to the source spectrum (Biviano et al. 1998c), as expected if they are indeed ghost images of the source. Some contribution to the ghost images from straylight from the background cannot be excluded at present.

Current modelling of the ISOCAM optical system is capable of explaining the origin, the positioning, and the extent of these ghost images, although some work remains to be done to understand their relative intensities (Okumura 1998b). Unfortunately, beyond the first order predictions of the model, the calibration observations have shown a more complicated behaviour of the ghost images, with a discontinuous variation in flux and position as the CVF position is changed.

It is clear that neglecting the ghost flux contribution induces an error of $\sim$ 30 % in the photometry of CAM sources. A similar figure is obtained for what concerns straylight, i.e. light incoming into the detector from outside the theoretical field-of-view. In particular, the straylight from the background affects CVF images by inducing a double-lobed pattern. Such a pattern makes it difficult to distinguish extended faint sources ($\leq$ 10 % of the background flux) in CVF images. Corrections for the straylight pattern in the CVF images has already been tried, based on CVF calibration observations of zodiacal background regions.

It is important to point out that the filter sensitiv values (see § 8) and SRF (see § 10) have been derived from aperture photometry corrected with a theoretical PSF, i.e. without including the flux from the ghosts. The observer should take care to avoid including the ghost flux in his photometric estimates, if he wants to assure consistency with the calibration sensitiv values. In cases where the source is extended, it becomes difficult to distinguish the source from the ghost contribution, so that a global overestimation of the total flux of $\sim$ 30 % can result.

It is clear that a global approach to modelling all these ghost/straylight effects is needed, and currently investigated (Okumura 1998b). Preliminary results (Okumura 1998b) are very promising.

Table 3: Filter-dependent relative positions of a point-source. Taken from Boulade (1996).

Filter	LW 1	LW 2	LW 3	LW 4	LW 5	
Y,Z position	15.0,15.0	15.0,16.0	15.0,14.5	15.0,14.0	16.0,14.0	
Filter	LW 6	LW 7	LW 8	LW 9	LW10	
Y,Z position	15.0,14.5	15.5,13.5	15.5,14.5	14.5,14.5	15.0,15.0	
Filter	SW 1	SW 2	SW 3	SW 4	SW 5	
Y,Z position	18.0,16.5	19.0,16.0	18.0,17.0	19.0,17.0	19.0,18.0	
Filter	SW 6	SW 7	SW 8	SW 9	SW10	SW11
Y,Z position	19.0,17.0	20.0,17.0	18.5,16.5	19.0,16.5	19.0,17.5	18.0,17.0

12 Pointing accuracy and astrometry

The analysis done by CIDT during the PV-phase (Boulade 1996) showed that there are 3 sources of error in the pointing accuracy:

- the tilt of the filters with respect to the optical axis (necessary to minimize ghost images);
- the Attitude and Orbit Control Subsystem;
- the jitter of the lens wheel.

By making a set of measurements of the same star, with different filters, but the lens wheel fixed in a given position, at the 1.5″PFOV, it was possible to determine the systematic displacement of the source on the detector depending on which filter is used. For instance, a star centered at the pixel 15,15 in the LW10 filter will fall on the pixel 19,18 in the SW5 filter. The position changes by up to 1.5 pixels in the Y-direction and 2.5 pixels in the Z-direction for different LW filters, and by up to 2 pixels in the Y-direction and 2 pixels in the Z-direction for different SW filters. The expected locations of a point source in the CAM fov for all filters are given in Table 3, taken from Boulade (1996). All positions are offset with respect to the position of a point source observed with LW10, which is set to (Y,Z)=(15,15) as a reference. The positions listed in Table 3 should be accurate to ≤ 0.4 pixels.

In the same analysis it was shown that the lens-wheel positioning jitter amounts to ± 2 pixels.

The pointing accuracy of the AOCS was determined through several observations done with CAM and SWS during revs.264, 368, 369. The analysis done by SIDT and CIDT (see Salama 1996a, and Salama 1996b) have shown that the typical RMS pointing accuracy was $\sim 3''$ in both the Y- and Z-direction before the star-tracker pointing accuracy was improved in rev.452, and it is now $\sim 2''$.

Thus, one expects a typical random error in the pointing of $2''(3'')$ after (before) rev.452 due to the AOCS, plus 2 pixels due to the lens-wheel jitter, to which one should add the systematic displacement due to the filter tilts.

This is confirmed by results of the OLP. More specifically, by looking at 61 measurements of several stars observed with many different CAM configurations, one can see that the average deviation of the position of a source from the expected position (in terms of given coordinates) is $\simeq 8''$with $\simeq 5''$RMS, on average, or, distinguishing among different PFOV's, 3″plus 3 pixels at the 1.5″and 3.0″PFOVs, 3″plus 2 pixels at the 6.0″PFOV, and 3″plus 1 pixel at the 12″PFOV (where the statistics, however, is quite low). Note that these values

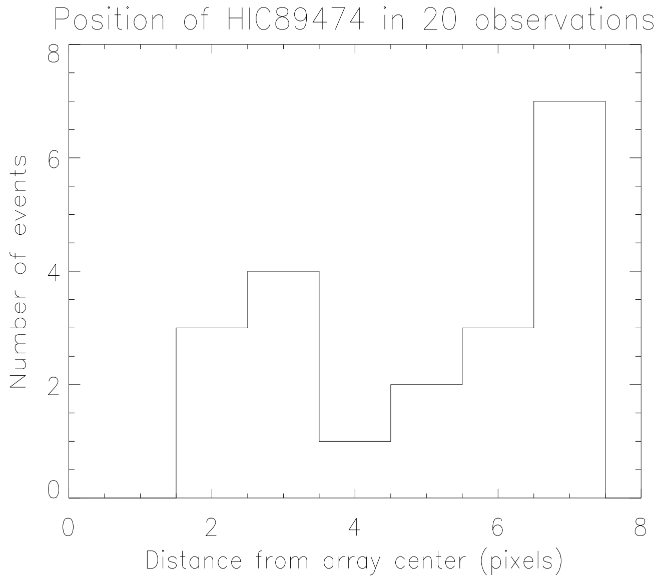

Figure 6: The histogram of the distances from the centre of the CAM array, in pixels, measured for the star HIC89474 in 20 observations done in different revolutions, with the same configuration (LW2 filter, 1.5″PFOV).

include the systematic displacements according to the filter used, and also the errors in the input coordinates of the observed star.

A further confirmation of the pointing accuracy of ISO-CAM comes from the observations of the star HIC89474, done during several revolutions, and always in the same configuration (LW2 filter, 1.5″PFOV). The histogram of the distances of the star from the centre of the array is shown in Fig.6. The average distance from the array centre is 2 pixels with an RMS of 1.

Note however that the relative pointing accuracy (i.e. the accuracy of pointings between two raster steps) is much better than the absolute pointing accuracy, and of the order of 0.1″(Aussel et al. 1998).

The most important astrometric limitation now comes from the lens wheel position jitter: the edge of the CAM 6″per pixel beam is sometimes displaced off the large Fabry-mirror, leading to a loss of signal on column 0, or sometimes column 31, of the array. This is also seen when the 3″PFOV is used in combination with the small Fabry-mirror (see Biviano et al. 1998a). The jitter results in an offset of more than one pixel from the optical axis (see, e.g., Aussel et al. 1998).

During the revolution 291, a star cluster has been observed with the purpose of providing an accurate geometry of the different optical channels (magnification and field distorsion). Results show that the CAM field distorsion is of pin-cushion type (see Aussel et al. 1998). The distorsion is bigger than a pixel at the edge of the field-of-view, at 6″PFOV. This affects the photometry of sources located at the edge of the array, as their flux is distributed over a larger area than it should be. This field distorsion has now been calibrated so that the CAM images can now be corrected for this effect. After correction, the s/n of sources at the edges of the array, increases by 50 %. Note however, that also the field distorsion correction suffers from the lens wheel position jitter.

Table 4: Summary of the error budget for CAM calibration.

Noise origin	magnitude	residual after correction
Stabilization (random)	10 $\times$ sky noise	2 $\times$ sky noise
Stabilization (systematic)	40 % source flux	15 % source flux
Saturation	$\geq$ 30 % decrease in responsivity	
Read-out noise	LW: 0.7 ADU/g	
	SW: 2 ADU/g	
Gain	0.15 % output current	
Dark current	LW: 0.5 ADU/g	0.25 ADU/g
	SW: 0.5 ADU/g	
Flat field	LW: 0.5 % (high background)	
	SW: $\leq$ 1 %	
Sensitiv	5 %	
PSF (photometric correction)	20 %	few %
PSF (pixel position)	$\leq$ 3 %	
CVF SRF	3 %	
CVF spectral purity	$\leq$ 1 CVF step	
Ghost	$\leq$ 30 %	
Straylight	10 % sky flux	
Astrometry (pointing)	$3''$	
Astrometry (jitter)	$\pm$1 column	
Astrometry (field distorsion)	1 pixel	

13 Conclusions

We summarize here the results of our analysis and comment upon them in the light of pre-launch expectations (Pérault et al. 1994; Pérault & Metcalfe 1995). In Table 4 we list the current estimates of the errors per each calibration field. When possible, we also give the error estimates after the application of suitable correction (like the stabilization routines described in § 2. These values are better explained in the following.

The contribution of glitches to the overall noise of CAM images is important, but efficient deglitching algorithms now exist. The main problem lies in the transient effects that certain (rare) glitches have in the pixel responsivities. It is because of these transient effects that glitches become an important source of noise.

In general, one can say that the dominant error source in CAM images is that due to transients. Unfortunately, transients contribute not only random error, but also systematic errors.

For what concerns random errors, algorithms like PRETI (Starck et al. 1998) and Lari's (Lari 1997) are able to reduce the stabilization noise. Pre-launch estimations indicated that the noise contribution from transient effects would be 2–3 times the Poisson noise (Pérault & Metcalfe 1995). This is indeed the level of accuracy that can now be obtained with the available algorithms (see, e.g. Fig. 3). Integrating long enough can also beat the stabilization noise, as it was shown in the very long FF calibration observations (Biviano et al. 1998a), but this was of course unfeasible in most normal observations.

As for the systematic errors induced by incomplete stabilization, the available routines allow to recover photometry to within $\pm$15 %. Without such corrections, however, the photometric results could be in error by $\sim$ 40 %. Again this is in line with pre-launch expectations. There is certainly room for further improving of the stabilization correction programs, so that the above given error estimate will certainly decrease in the future.

Saturation is possibly an extreme case of long stabilization noise. Whenever an observation is affected by saturation, the strong decrease in pixel sensitivities ($\geq$ 30 %) seriously affects photometry. Fortunately, saturation events have been kept to a minimum by the careful work of several people.

The gain accuracy is very good, and gain scaling does not indtroduce any significant errors in the reduced data.

The dark current calibration is now very well constrained thanks to the accurate temporal model developed by Biviano et al. (1998b) for the LW detector. Both the LW and the SW detector dark-current calibration provide residuals (after subtraction) close to the pre-launch estimations of 0.3 ADU/g and 0.5 ADU/g, resepctively (the LW dark-current residual is actually even slightly lower). Failing to account for the temporal drift of the dark-current would have increased the LW dark-current noise by a factor 2.

Incomplete stabilization is an issue for the flat-field measurements. Based on a single PV-phase very long flat-field observation, we have concluded that a large part of the small residual error in our flat-field observations is due to incomplete stabilization. However, reducing the noise by a further 0.5 % (from the 0.5 % accuracy reached for the LW10 6″flats) would imply observing 5 times longer. This is maybe achievable for some configurations, and indeed we already have such long observations for two configurations (LW10 and LW3 6″).

However, we stress that our strategy for measuring flat-fields was well adapted to the behaviour of the flat-field, since most of the stabilization noise arises from the first 800 s observation (and we are typically observing twice as long). The noise levels we are reaching are in some cases lower than expected pre-launch (1 % in LW and 3 % in SW). In Table 4 we quote the 0.5 % accuracy reached in the highest background flux filter (LW10), since it is the product of the background flux times the accuracy which matters for the source detection and photometry.

Repeated observations of the same star through several revolution has shown that the photometric calibration is stable, to within a few per cent. The main source of scatter is probably due to transient effects which however are not extremely important for our high flux calibrating stars. Another source of scatter in the photometry is the decrease in reponsivity through the orbit, -6 % in total. The sensitiv parameters are accurate to within $\sim$ 5 %, on average, and do not differ very much from the pre-launch values. The accuracy looks however a little bit worse than expected pre-launch (2 %), but this is due to the fact that the measured photometry is PSF corrected, so the sensitiv error estimates include the uncertainty in the PSF.

The observed PSF is generally quite close to the theoretical one, except for the cases where the ghost contribution is significant. The theoretical PSF can then be used for photometry correction without a significant loss of accuracy. However, the accuracy of observed PSFs does not allow deconvolution yet. This may be due to poor sampling and/or incomplete stabilization, that is very difficult to achieve, though. Clever algorithms could prove succesfull in this respect.

The CVF Spectral Response Function is very well constrained at (almost) all wavelengths. This is proven by the impressive agreement of the observed spectrum of γ Draconis with the independent measurements of Cohen et al. (1995). Typically, the SRFs are accurate to 3 % RMS on average. However, CVF images are affected by ghost and straylight to a significant level. Whenever the ghost cannot be separated by the source image, and its flux cannot be estimated, the photometric accuracy can be affected by up to 25 %. Also straylight from sources outside the theoretical field-of-view can affect CVF images to an extent that extended sources with a flux below 10 % of the background are not detectable.

Wavelength calibration of the CVF is very accurate when the source is located at the centre or on the right part of the array, but suffers from a systematic shift to longer wavelengths when the source is imaged in the left part of the array (of up to 1 CVF step position).

Ghost-images may contain ~ 30 % of the source flux; it is therefore important to calibrate photometry accordingly. All sources have so far been calibrated without including the flux in the ghost. At least two kinds of ghost-images have been identified, and proper characterization of their location, size, and shape is important for a clean imaging of faint structures. A detailed modelling of the instrument + telescope optics, including the transmission and reflection coefficients of the detector and filter surfaces, is currently being produced, with very promising preliminary results.

For what concerns the astrometric accuracy, CAM observations have been done to improve the ISO pointing accuracy to a level of $\sim 3''$RMS, and the CAM pin-cushion field distorsion has been modelled and it is now corrected, allowing an increase in s/n of sources located at the edge of the CAM array. Currently, the main limitation in the astrometric accuracy comes from the lens wheel jitter, displacing the beam off the Fabry-mirror and inducing a loss of signla in the edge columns of the detector.

We conclude by pointing out that, given the large number of CAM configurations, the vaste amount of calibration topics to be addressed, and the limited calibration observing time, the CAM calibration strategy had to be a success-oriented strategy. This comparison with pre-launch expectations shows that this strategy has proven to be essentially valid.

References

Abergel A., Désert F.-X., Aussel H. 1996, “IAS Model for ISOCAM LW Transient Correction”

Aussel H., Cesarsky C., Elbaz D., Starck J.-L. 1998, *AA,* submitted.

Biviano A. et al. 1998a, “The ISOCAM flat field calibration report”

Biviano A. et al. 1998b, “The ISOCAM dark current calibration report”

Biviano A. et al. 1998c, “The ISOCAM CVF calibration report”

Blommaert J. 1998, “ISOCAM Photometry Report”

Boulade O. 1996, "CAM Report on Pointing Jitter”

Claret A. & Dzitko H. 1998, “ISOCAM glitch library”

Delaney M. 1997, “ISOCAM interactive analysis user’s manual”, v.2.0

Gallais P. 1996, “About the saturation with CAM” – Contribution to the ISOCAM Calibration Review

Gallais P. 1998, “Report on the Trend Analysis of the CAM Daily Calibration Measurements”

Lari C. 1997, “IRA model for ISOCAM LW transient correction”

Laurent O. et al. 1998, “ISOCAM observation of the ultraluminous galaxies IRAS19254-7245, IRAS23128-5919, and IRAS14348-1447” (in preparation)

Okumura K. 1998a, “ISOCAM PSF Report”

Okumura K. 1998b, “Ghosts in ISOCAM images”

Ott S. et al. 1996, “Design and implementation of CIA, the ISOCAM interactive analysis system”, ASP conference series vol.125

Pérault M. et al. 1994, *Optical Engineering,* 33, 762

Pérault M., Metcalfe L. 1995, “Technical Note About the Error Budget Estimate in CAM Observations”

Salama A. 1996a, "Report on the Rev.264 ISO Pointing Accuracy Experiment”

Salama A. 1996b, "The Rev.368/369 ISO STR Calibration Adjustement Verification Experiment”

Siebenmorgen R., Starck J.-L., Cesarsky D.A., Guest S., Sauvage M. 1998, “ISOCAM data user’s manual”

Starck J.-L. et al. 1998, in "Extragalactic Astronomy in the Infrared", p.481, eds.: G.A. Mamon, T. Xuân Thuân, J. Trân Thanh Vân, Editions Frontières (Paris)

List of abbreviations and symbols

- ADU - Analog to Digital Unit, the unit of all CAM observations;
- CVF - Circular Variable Filter;
- DF - Detector Flat;
- FF - Flat Field;
- g, G - Gain;
- ICD - Internal Calibration Device;
- OF - Optical Flat;
- PFOV - Pixel Field-Of-View;
- PSF - Point Spread Function;
- s, sec - second, unit of time;
- T_{int} - the integration time of a single frame exposure;